





Contents lists available at CEPM

Computational Engineering and Physical Modeling

Journal homepage: [www.jcepm.com](http://www.jcepm.com)



## Numerical Analysis of Segmental Tunnel Linings Employing a Hybrid Modeling Approach

A. Granitzer <sup>\*</sup>, F. Tschuchnigg 

Institute of Soil Mechanics, Foundation Engineering and Computational Geotechnics, Graz University of Technology, Austria

Corresponding author: [andreas-nizar.granitzer@tugraz.at](mailto:andreas-nizar.granitzer@tugraz.at)

 <https://doi.org/10.22115/CEPM.2021.247314.1130>

### ARTICLE INFO

#### Article history:

Received: 08 September 2020

Revised: 10 January 2021

Accepted: 05 January 2021

#### Keywords:

3D finite-element analysis;

Tunnel;

Segmental lining;

Joint stiffness;

Tunnel heave.

### ABSTRACT

The structural performance of shield-driven tunnel linings is considerably affected by the existence of segmental joints. Nevertheless, segmental tunnel linings are commonly modelled as isotropic structures in engineering practice, thereby ignoring the joint-induced stiffness reduction in numerical analysis. A more realistic approach is to consider the tunnel structure as continuous ring with adjusted rigidities which is also referred to as indirect-joint model. However, this modeling approach is a complicated task since it requires the definition of anisotropic stiffness parameters. In this context, the present paper introduces a hybrid modeling approach, which combines analytical solutions and numerical studies. Based on extensive numerical studies, anisotropic stiffness parameters are defined to model an existing drainage tunnel (SDT). Finally, a case study is discussed, where the developed indirect-joint model is used to investigate the structural response of the SDT. In this context, particular emphasis is placed on the deformation of the tunnel crown developing throughout the entire construction phase.

How to cite this article: Granitzer A-N, Tschuchnigg F. Numerical Analysis of Segmental Tunnel Linings employing a Hybrid Modeling Approach. *Comput Eng Phys Model* 2021;4(1):1–18. <https://doi.org/10.22115/cepm.2021.247314.1130>

2588-6959/ © 2021 The Authors. Published by Pouyan Press.

This is an open access article under the CC BY license (<http://creativecommons.org/licenses/by/4.0/>).



## 1. Introduction

In the latter half of the 20<sup>th</sup> century, mechanical tunnel driving has made remarkable progress. A brief overview of respective tunnelling machines and their applicability is given in [1]. As a consequence, shield-driven tunnelling methods are nowadays widely adopted for the construction of urban underground tunnels and, in many cases, provide several advantages such as cost effectiveness, a minimum impact on ground traffic and surface structures as well as flexibility compared to the conventional tunnelling method. This holds particularly true for soft soil conditions [2]. Moreover, shield driven tunnel linings are segmented and represent an assembly of prefabricated reinforced concrete segments. A general differentiation can be made between linings with flat joints (straight-jointed assembly) and linings with offsets (stagger-jointed assembly) [3]; see Fig. 1 left. Each ring consists of a set of concrete segments which in turn interact via segment-to-segment interfaces. The latter are herein referred to as longitudinal joints. In contrast, the interaction between concrete segments of adjacent rings is established via ring-to-ring-interfaces which are denoted as ring joints; see Fig. 1 right.

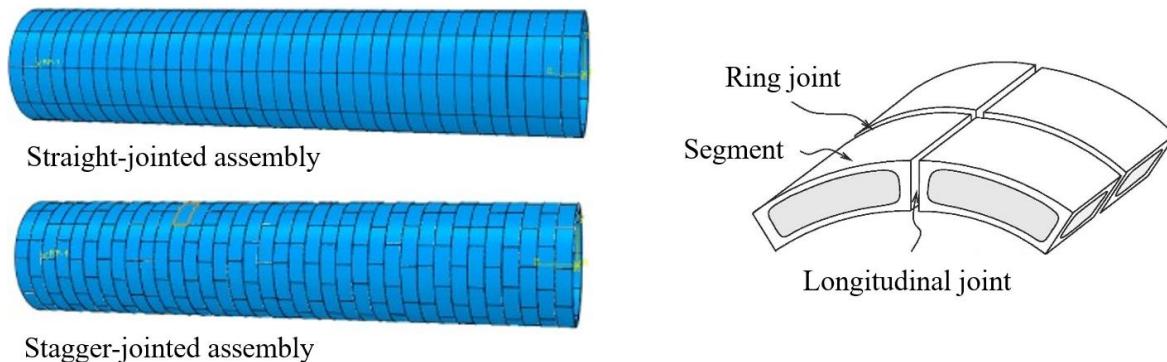


**Fig. 1.** Definition of lining components [4] (left) and assembly configurations [5] (right).

In general, the lining can fail due to both, failure of the tunnel lining itself or as a consequence of failure of the soil behind the lining. To prevent failure of the lining, several design requirements and quality standards have to be considered. It is noted that the latter concern not only loading conditions subsequent to the lining installation process, but also transportation and installation [6]. Furthermore, large deformation effects due to excessive flattening have to be considered, which may invoke significant second order bending moments [7]. If the latter exceed the bending-moment-reducing effect of the activated ground resistance next to the lining, second order bending moments may govern the lining design as they increase until the ultimate bearing capacity is reached [8]. Further information on damage mechanisms related to tunnel linings are given in [9].

In engineering practice, segmental tunnel linings are commonly approached as isotropic rings, thus ignoring the jointed configuration. However, since construction joints substantially affect the structural response of geotechnical structures resulting in a decreasing rigidity of the overall structure, they are expected to behave anisotropic rather than isotropic [10,11]. The latter particularly applies for shield tunnel linings since they are separated by joints in two directions [12]; ignoring them may lead to a conservative design. On the contrary, overestimating the

influence of joints and consequently reducing the stiffness of a tunnel structure extensively could result in unrealistic deformations, which might lead to a misinterpretation of the waterproofness [13]. To improve the current practice, advanced design approaches should be applied, where the peculiarities of segmental tunnel linings are taken into account.

The present paper aims to quantify the influence of joints on the structural behaviour of segmental tunnel linings. To investigate this problem 3D finite element analysis (FEA) have been performed, where the lining is modelled as plate element with anisotropic material behaviour. This approach is also referred to as indirect-joint model [14]. In order to derive reasonable anisotropic stiffness parameters representing the behaviour of the tunnel lining as realistic as possible, a hybrid modeling approach is introduced, which combines numerical parameter studies and well-accepted analytical formulations. For the presented studies an existing shield-driven tunnel, which serves as drainage tunnel of a suburban area in Europe, is used as reference structure.

The paper is structured as follows. Section 0 provides a brief overview of the methods to model tunnel linings. Section 3 presents the basic workflow of the hybrid modeling approach; a detailed description is given in [15]. In section 0, the proposed conceptual framework is deployed, where the SDT serves as reference structure. Section 0 discusses 3D FEA of a recent suburban construction project where the existing SDT was subjected to effects resulting from an above-crossing tunnel. For the case study, selected aspects of the numerical calculations are highlighted whereas particular emphasis is placed on the deformation of the tunnel crown developing throughout the construction phase. Section 0 contains the conclusions drawn based on the results of the presented analyses.

All results discussed in this paper are computed with the finite element codes of PLAXIS. The numerical calculations were conducted with the versions PLAXIS 2D 2018.01 [16] and PLAXIS 3D 2018.01 [17].

## **2. Methods to model tunnel linings**

Regarding the design of segmental tunnel linings, three categories exist: empirical methods, analytical solutions and numerical methods [18]; an overview is found in [19]. In any method, the joint configuration substantially governs the structural response. To take these effects into account, the joint-related behaviour of segmental tunnel linings can either be approached as indirect-joint or direct-joint model. Indirect-joint models consider lining structures as uniform rings with adjusted rigidities due to the construction joints; on the contrary, construction joints are explicitly modelled in direct-joint models [20]. Furthermore, a distinction has to be made between two loading modes imposed by the surrounding soil, namely the active-loading mode and the passive loading mode. For the active loading mode, the load acting on the lining is calculated by empirical or analytical formulas, for the passive loading mode, the load acting on the lining is calculated taking into account the soil-lining interaction by means of displacement compatibility [21].

In case of indirect-joint modeling of the cross-section, the effect of joints can be considered in the analysis assuming an indirect proportional relationship between the number of longitudinal joints and the circumferential bending rigidity as given in Equation (1) [22]:

$$I_L = \left[ \frac{4}{N} \right]^2 \cdot I_0 + I_j < I_0 \quad (1)$$

where  $N$  is the number of concrete segments per ring ( $N > 4$ ),  $I_0$  is the moment of inertia of the concrete segments per unit length of a segmental tunnel and  $I_j$  is the moment of inertia at the longitudinal joints per unit length of a segmental tunnel. During the last decades, this formulation was modified by several researchers, whereas additional influencing factors such as joint distribution or subgrade modulus  $K_s$  were taken into consideration [2]. In this context, the effective transversal bending rigidity ratio  $\eta$  was introduced (Equation 2) [23]:

$$\eta = \frac{(EI)_{c,jointed}}{(EI)_{c,continuous}} \leq 1 \quad (2)$$

where  $(EI)_{c,jointed}$  marks the effective flexural rigidity of the jointed ring structure and  $(EI)_{c,continuous}$  is the flexural rigidity of the equivalent continuous ring structure in circumferential direction. Analogously, the concept of the effective longitudinal bending rigidity ratio  $\xi$  was established (Equation 3) [24]:

$$\xi = \frac{(EI)_{l,jointed}}{(EI)_{l,continuous}} \leq 1 \quad (3)$$

where  $(EI)_{l,jointed}$  marks the effective flexural rigidity of the jointed ring structure and  $(EI)_{l,continuous}$  the flexural rigidity of the equivalent continuous ring structure in longitudinal direction. Different to the effective transversal rigidity ratio,  $\xi$  addresses a reduced flexural rigidity in the longitudinal direction due to the presence of ring joints. By taking  $\xi$  into account, the response of the lining in longitudinal direction can take two deformation modes approximately into consideration, namely the bending deformation mode and the deformation mode of dislocation; see Fig. 2. A comprehensive list of calculation models concerning the longitudinal response of shield tunnels is given in [25].

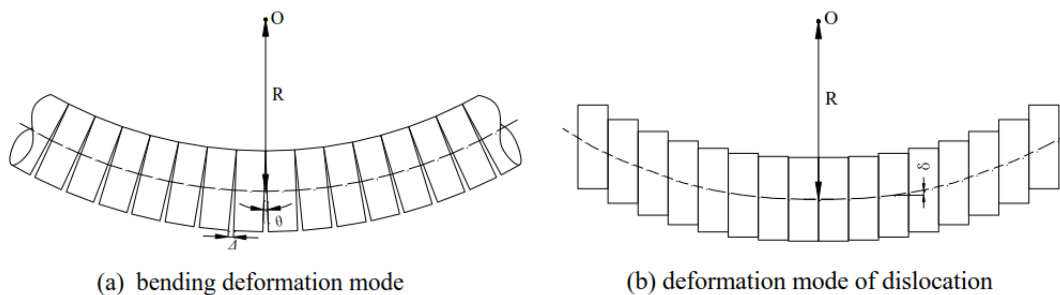


**Fig. 2.** Longitudinal deformation modes [25].

So far, the transverse and longitudinal behaviour of segmental tunnel linings have been approached as two-dimensional problems, though it is a three-dimensional boundary value problem. Particularly, because the longitudinal and the transverse stiffness of a liner are related to each other [4]; this effect was also shown by [26]. In this context, parametric studies were

performed which indicate that the longitudinal bending stiffness of the segmental liner increases with the transverse bending stiffness of the tunnel cross-section. In [26] it is also shown that longitudinal differential settlements lead to additional tangential bending moments due to flattening; unless this is taken into account, the design might be unsafe[7]. Further investigations presented in [27] were performed addressing the longitudinal load transfer mechanism of tunnel linings by means of a cylindrical shell within an elastic foundation. These calculations led to the conclusion that both, an increase of circumferential and radial stiffness results in a decreasing bending moment in the cross-section of a tunnel lining. Hence, structural measures should be taken to strengthen the shear stiffness between rings in order to reduce the additional bending moment induced by ground displacements. In [27], 3D effects of relevant results are highlighted, which are only insufficiently captured by 2D analyses. As a consequence, the authors concluded that 3D FEA are highly recommended to assess the structural behaviour of segmental tunnel linings. Therefore, the subsequent chapter presents a modeling framework using 2D and 3D FEA, which allows to evaluate the effects of joints on the (three-dimensional) behaviour of segmental tunnel linings. However, main emphasis is put on the derivation of modeling parameters in order to capture the structural behaviour as realistically as possible.

### 3. Hybrid modeling approach - Workflow

This section introduces a hybrid modeling approach combining both, analytical formulations and numerical results. Therefore, the existing SDT lining, which is modelled as plate element with anisotropic material (indirect-joint model), serves as reference structure. In order to account for the effects of segmental joints on the lining behaviour, the bending stiffness  $E \cdot I$ , the normal stiffness  $E \cdot A$  as well as the shear stiffness  $G \cdot A$  have to be adapted; Fig. 3 illustrates the basic idea of the joint-induced stiffness reduction.

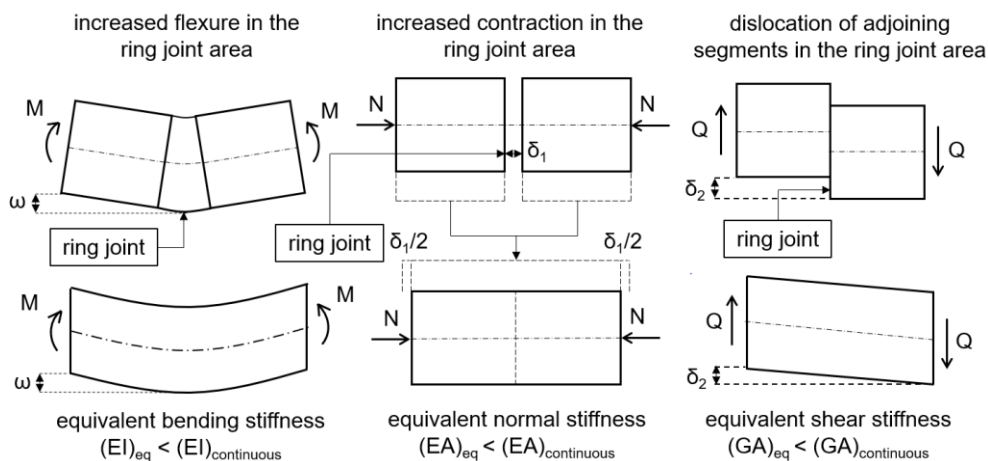


**Fig. 3.** Basic idea of the joint-induced stiffness reduction in longitudinal direction.

For a given plate thickness  $d$ , the effective material cross section areas for both, shear forces and normal forces, represent constants, the same applies for the moment of inertia against bending. Thus, the geometric properties cannot be modified in order to reduce  $E \cdot I$ ,  $E \cdot A$  and  $G \cdot A$  to model the effects of joints. Hence, to model the joint-induced stiffness reduction an adjustment of the

anisotropic stiffness parameters  $E_1$ ,  $E_2$ ,  $G_{12}$ ,  $G_{13}$  and  $G_{23}$  (see Fig. 4) is required. In other words, geometric anisotropy is approached as material anisotropy. In this context, several recommendations are reported in the literature with respect to the modeling of T-shaped floor profiles, sheet-pile walls and retaining walls [10,11,28]. The present study extends the basic idea of the joint-induced stiffness reduction to model segmental tunnel linings, thereby addressing the following questions:

- How do longitudinal joints affect the cross-sectional behaviour?
- How can ring joints be taken into consideration by means of an indirect-joint model?
- To which extent is the max. cross-sectional bending moment influenced by the joint-induced shear stiffness reduction?

To investigate the problem and to answer the questions, a five-step procedure is established, which also allows to determine the anisotropic stiffness parameters of a segmental tunnel lining (i.e.  $E_1$ ,  $E_2$ ,  $G_{12}$ ,  $G_{13}$ ,  $G_{23}$ ). In the following, a brief description of each step is given; a detailed description is given in [15]. However, the key results are reported in the subsequent section. The SDT serves as reference structure for all studies discussed in the following.

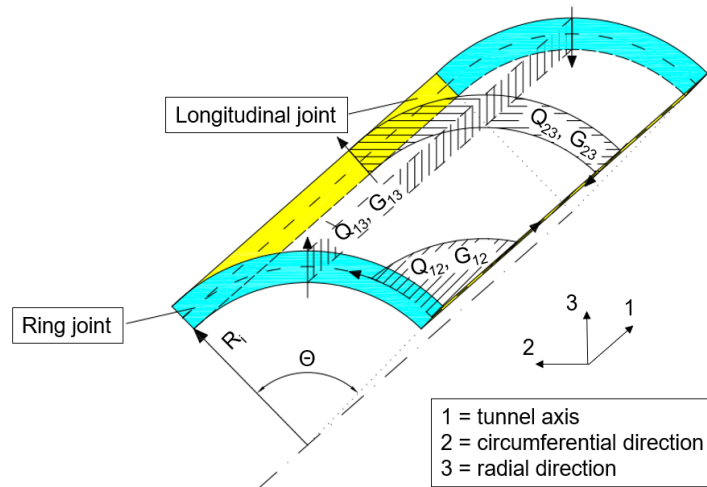


Fig. 4. Orientation of shear forces, shear moduli and shear deformations.

### Step 1: Simplification of SDT geometry

The considered drainage tunnel represents a stagger-jointed ring assembly formed by hexagonal concrete segments with no plane of symmetry present. For the following studies, the investigated tunnel geometry has been simplified as illustrated in Fig. 5 left.

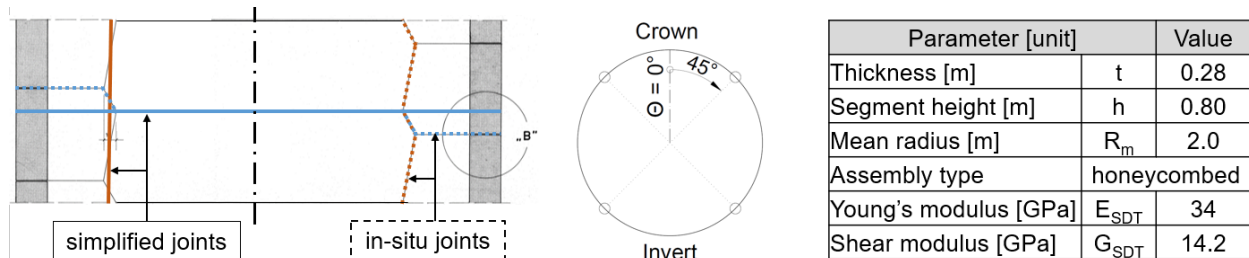
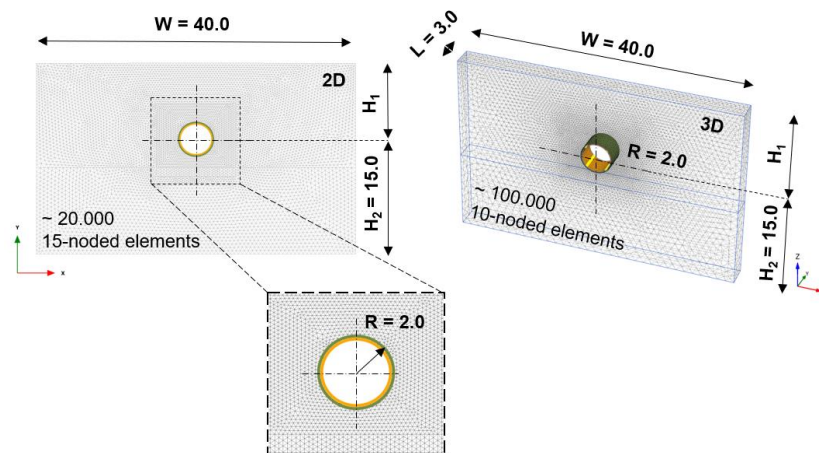


Fig. 5. Simplified geometry (left); SDT-parameters (right).

In the FEA, both, the longitudinal and the ring joints are approximated as flat joints, which extend parallel and perpendicular to the tunnel axis, respectively. In other words, the present stagger-jointed lining assembly is considered as straight-jointed lining assembly. With respect to the longitudinal deformation behaviour of a four-fold segmented tunnel lining, the eligibility of this simplification approach is strengthened by [22,26].

### Step 2: Examination of cross-sectional structural behaviour

Based on the simplified cross-section, 2D as well as 3D calculations are conducted where a differentiation is made between loading and unloading conditions. The 3D models are generated by extending the 2D geometries by three metres in the third dimension. While shape functions of fourth order are used for the majority of the 2D calculations, quadratic shape functions are used for some FEA for reasons of comparison between 2D and 3D (offers only shape functions of second order). In this way, it is possible to evaluate differences based on geometrically equivalent models in 2D and 3D. Fig. 6 shows both, the model dimensions and the mesh discretization of the boundary value problem. With regard to longitudinal-joint-modeling, the rotational rigidity  $K_{RO}$ , which is defined as the bending moment-per-unit length required to develop a unit rotation angle along the joints of the assembled segments, lies somewhere between the extreme values for ideally rigid and ideally hinged joints. Hence, finite element analyses are conducted in which the rotation degrees of freedom (i.e. representing longitudinal joints) are modelled as rigid and fully hinged, respectively. In an additional analysis, the SDT is modelled as uniform ring without joints as well. However, the translational degrees of freedom remain fixed in all calculations. It is further noted that the model depth is not constant and varies for loading and unloading conditions. With these models, deviations resulting from different longitudinal joint modeling approaches are investigated. The derived findings are then used to determine the transversal bending rigidity ratio  $\eta$  of the SDT.



**Fig. 6.** Uniform ring model - 2D finite element mesh (left); 3D finite element mesh (right).

### Step 3: Examination of the longitudinal structural behaviour

In this step, the drainage tunnel is modelled as continuous circular 3D plate element with anisotropic material, thereby taking into account the effect of both, longitudinal joints and ring joints on the lining behaviour. Considering the influence of longitudinal joints, the effective

transversal bending rigidity ratio  $\eta$ , which is deduced from step 2, is used to modify both the normal stiffness ( $E_2 \cdot A_2$ ) and the bending stiffness ( $E_2 \cdot I_2$ ) in circumferential direction as follows:

$$E_2 \cdot I_2 = E_{SDT} \cdot \eta \cdot \frac{t^3 \cdot 1m}{12} \quad (4)$$

$$E_2 \cdot A_2 = E_{SDT} \cdot \eta \cdot t \cdot 1m \quad (5)$$

where  $I_2$  is the moment of inertia against bending over the longitudinal axis,  $A_2$  is the effective material area for axial forces in the circumferential direction,  $E_2$  is the effective Young's modulus in the circumferential direction and  $E_{SDT}$  is the Young's modulus of the SDT concrete segments; see Fig. 5 right. Regarding the presence of ring joints, both, the normal stiffness ( $E_1 \cdot A_1$ ) and the bending stiffness ( $E_1 \cdot I_1$ ) in longitudinal direction are modified according to [29]. Therefore, an analytical solution is used to quantify the longitudinal bending rigidity ratio  $\xi_{Cont.}$ :

$$E_1 \cdot I_1 = E_{SDT} \cdot \xi_{Cont.} \cdot \frac{t^3 \cdot 1m}{12} \quad (6)$$

$$E_1 \cdot A_1 = E_{SDT} \cdot \xi_{Cont.} \cdot t \cdot 1m \quad (7)$$

In the Equations (6-7),  $I_1$  is the moment of inertia against bending over the circumferential axis,  $A_1$  is the effective material area for axial forces in the longitudinal direction,  $E_1$  is the effective Young's modulus in the longitudinal direction and  $E_{SDT}$  is the Young's modulus of the SDT concrete segments.

#### Step 4: Model transformation

The previous steps focus on the joint-induced reduction of the normal stiffness as well as the bending stiffness. In addition, segmental joints also affect the shear stiffness  $G \cdot A$  [27]. However, indirect-joint models have shortcomings regarding the investigation of complex joint characteristics such as the joint-induced shear stiffness reduction. To overcome this limitation and to investigate the effect of joints on  $G \cdot A$ , the indirect-joint model used in step 3 is transformed to the direct-joint model as illustrated in Fig. 7 left. For the direct-joint model, the following two assumptions are made:

- Longitudinal joints have a minor effect on the rigidity of the lining, if the number of segments is less or equal four [22]. Hence, the segmental lining is approached as a series of uniform isotropic rings ( $L_{segment} = 0.52$  m) separated by ring joints ( $L_{joint} = 0.28$  m), whereas the latter is assumed to be equal to the lining thickness.
- Ring joints are modelled as thin plate sections. In this way, both a reduced longitudinal bending stiffness  $(E_1 \cdot I_1)_{Joint}$  and a reduced normal stiffness  $(E_1 \cdot A_1)_{Joint}$  of the ring joint area compared to the adjacent isotropic rings is accounted for. In contrast to the indirect-joint model, in which both stiffness components are uniformly reduced along the entire tunnel length, the direct-joint model restricts the influence of the ring-joint-induced stiffness reduction to the ring joint area. Consequently, the impact of the ring-joint-induced shear stiffness reduction can be studied in more detail.

To provide consistency between both models, comparative 3D calculations were conducted in which the vertical deformations occurring at the crown were chosen as matching parameter; the



model dimensions are shown in Fig. 7 right. Consequently, the longitudinal bending rigidity ratio of the ring joint area  $\xi_{\text{Joint}}$  is selected such that the vertical deformations at the crown show good agreement amongst both models.

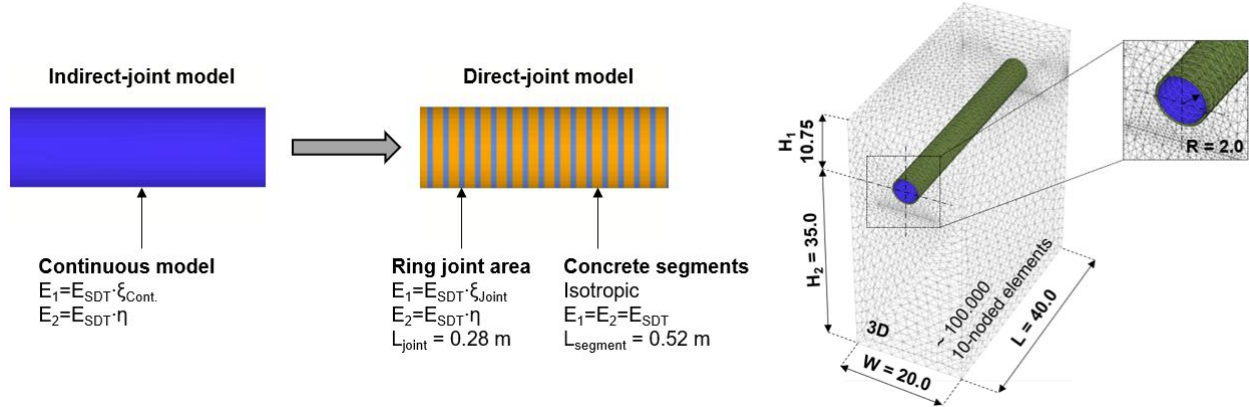


**Fig. 7.** Model transformation - indirect-joint and direct-joint model (left); 3D finite element mesh (right).

### Step 5: Analysis of joint-induced shear stiffness reduction

Based on the calibrated direct-joint model, step 5 aims to get a better understanding of the consequences of the joint-induced shear stiffness reduction. In order to account for the shear-induced offsets at the ring joints, the translational movements are approximated as shear deformation of the thin plates representing the ring joints; see Fig. 8. Correspondingly,  $(G_{12} \cdot A_{12})_{\text{Joint}}$  and  $(G_{13} \cdot A_{13})_{\text{Joint}}$ , that determine the shearing behaviour in the ring joint area, are reduced by employing a parameter called shear stiffness reduction ratio  $\zeta_{\text{Joint}}$ :

$$\zeta_{\text{Joint}} = \frac{(G \cdot A)_{\text{Joint}}}{(G \cdot A)_{\text{SDT}}} \leq 1 \quad (8)$$

where  $(G \cdot A)_{\text{Joint}}$  is the effective shear stiffness of the ring joint area in the direction of the respective axes  $(G_{12} \cdot A_{12})_{\text{Joint}}$  or  $(G_{13} \cdot A_{13})_{\text{Joint}}$  and  $(G \cdot A)_{\text{SDT}}$  is the shear stiffness of the SDT concrete segments.

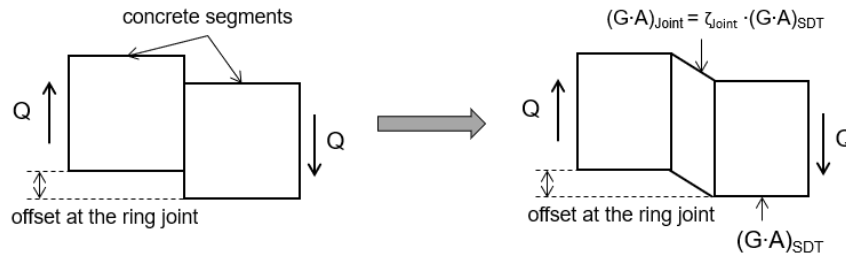


**Fig. 8.** Modeling approach to account for the ring-joint-induced shear stiffness reduction.

The effective material cross section area for both, the shear force  $Q_{12,\text{Joint}}$ ,  $A_{12,\text{Joint}}$ , as well as for the shear force  $Q_{13,\text{Joint}}$ ,  $A_{13,\text{Joint}}$ , represent constants for a given plate thickness  $d$ . Hence, slipping at the ring joints is taken into consideration by reducing the corresponding shear moduli  $G_{12,\text{Joint}}$  and  $G_{13,\text{Joint}}$  as follows:

$$G_{12,\text{Joint}} = G_{\text{SDT}} \cdot \zeta_{\text{Joint}} \quad (9)$$

$$G_{13,Joint} = G_{SDT} \cdot \zeta_{Joint} \quad (10)$$

To analyse the effect of the ring-joint-induced shear stiffness reduction on the SDT concrete segments, six sets of coefficients ( $\zeta_{Joint} = 0.01, 0.05, 0.1, 0.3, 0.5, 1.0$ ) are adopted in this study. These results allow to assess the effect of the joint-induced shear stiffness reduction on both, the SDT deformation behaviour and the max. cross-section bending moment  $M_{max}$ , which is, in turn, significant for the design of the concrete segments.

## 4. Hybrid modeling approach - Numerical parameter study

This section captures key observations of the numerical studies which were conducted by means of 2D and 3D FEA; in this context, loading as well as unloading conditions were considered. Since the present paper concerns the practical application of the hybrid modeling approach rather than modeling details, the reader is referred to [15] regarding further details of the performed analysis.

### 4.1. Effect of longitudinal joints on cross-sectional behaviour

Concerning step 2 of the hybrid modeling approach, the development of bending moments around the circumference of the lining is investigated in the following. Therefore, the effect of rotational rigidity  $K_{RO}$  is evaluated. In order to deduce more general statements, different loading intensities are considered in the FEA. The results shown in Fig. 9 represent upper and lower boundary values with respect to the possible bending moment  $M$  since they constitute extreme  $K_{RO}$ -values (i.e. rigid, fully hinged, uniform ring). The results clearly demonstrate that the rotational rigidity does not affect the distribution of bending moments around the circumference of the tunnel in both investigated loading cases. Likewise, the 2D results show good agreement with those obtained from the corresponding 3D models provided that quadratic shape functions are used; see Fig. 10. The results show that the jointed cross section can be approached as uniform ring corresponding to a  $\eta$ -value of 1.0, which is in accordance with the findings presented in [22].

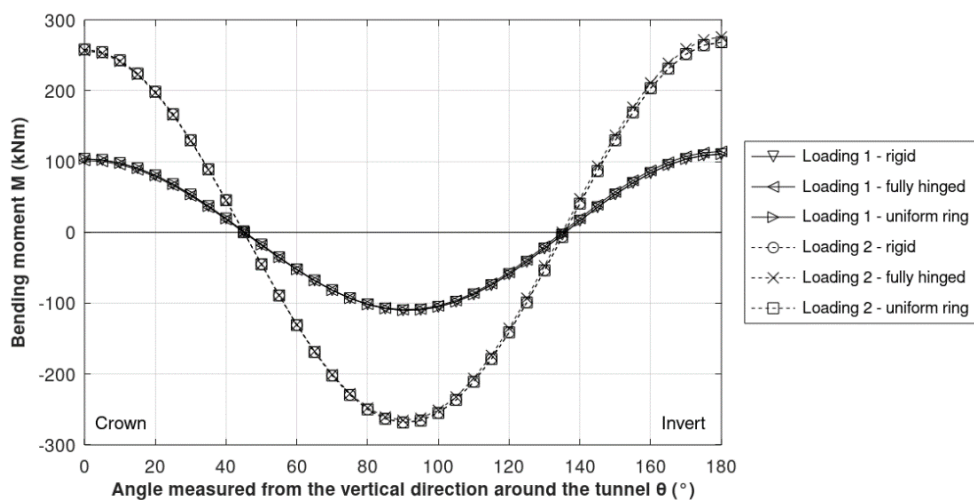


**Fig. 9.** Bending moments considering different joint configurations and loading conditions (2D).

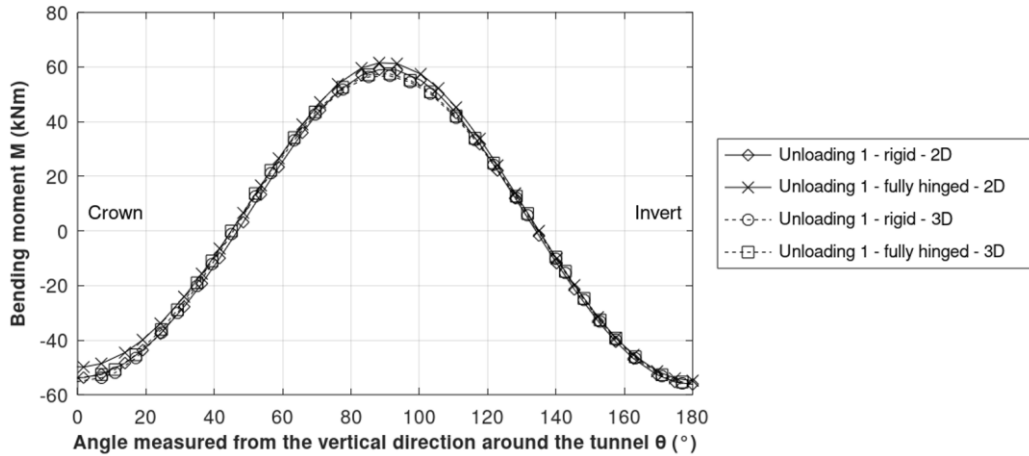


**Fig. 10.** Bending moments considering different joint configurations (unloading conditions).

Based on the FEA, the SDT structure can therefore be considered as a series of concrete segments separated by ring joints. However, the following assumptions were made for the performed studies:

- Symmetrical (un)loading conditions
- Straight-jointed lining assembly
- Ring geometry composed of four segments
- No slipping of adjoining concrete segments at the longitudinal joints

#### 4.2. Modeling of longitudinal structural behaviour

As described in step 3 of the hybrid modeling approach, the analytical solution proposed by [29] is used to quantify the ring-joint-induced stiffness reduction in longitudinal direction by means of the longitudinal bending rigidity ratio  $\xi_{\text{Cont.}}$ ; Table 1 summarizes the SDT-related input data required to determine  $\xi_{\text{Cont.}}$ .

**Table 1**

SDT-related input data required to determine  $\xi_{\text{Cont.}}$ .

Parameter [unit]		Value
Segmental length [m]	$L_S$	0.8
Young's modulus [GPa]	$E_S$	34
Number of longitudinal bolts [-]	$n$	8
Translational bolt stiffness [MN/m]	$K_b$	105
Cross section area [m <sup>2</sup> ]	$A_S$	3.5
Influence length of ring joint [m]	$L_f$	varied

Due to the fact that there is no information about the influence length  $L_f$  of the present ring joint, a sensitivity study was first conducted to investigate its effect on  $\xi_{\text{Cont.}}$ . The longitudinal bending rigidity ratio decreases with increasing  $L_f$ -values, whereas  $\xi_{\text{Cont.}}$  remains almost constant for  $L_f$ -values greater than 0.05 m; see Fig. 11. Since the flexural rigidity of jointed ring structures is lower compared to equivalent continuous ring structures, the observed tendency is reasonable; accordingly,  $\xi_{\text{Cont.}}$  reaches its maximum if the ring joints disappear ( $L_f = 0$  m).

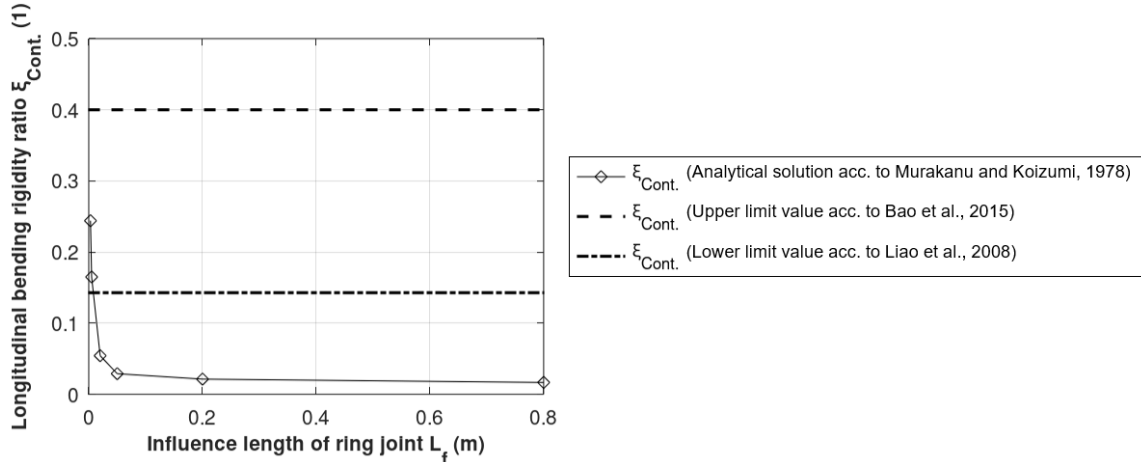


**Fig. 11.** Relationship between influence length of ring joint  $L_f$  and longitudinal bending rigidity ratio  $\xi_{Cont.}$ .

In Fig. 11, [26] and [27] serve as guideline to mark a typical range of  $\xi_{Cont.}$ -values considered for segmental tunnel linings (i.e. 0.14 and 0.40). In the present case, the influence length of the ring joint is defined as  $L_f = 3$  mm which corresponds to the SDT ring joint thickness. Based on the analytical solution, this gives a  $\xi_{Cont.}$ -value of 0.24 which falls within the range of typical values as shown in Fig. 11.

#### 4.3. Influence of shear stiffness reduction on max. cross-sectional bending moment

In order to study the consequences of a joint-induced shear stiffness reduction, the indirect-joint model is transformed into a direct-joint model; see Fig. 7. To provide consistency between both models, the vertical crown displacements developing in longitudinal direction are used for calibration purposes. Preliminary studies showed that the direct-joint model is in good agreement with the structural behaviour of the indirect-joint model ( $\xi_{Cont.} = 0.24$ ) if  $\zeta_{Joint}$  is set to 0.10 for both, loading and unloading conditions; see also [15].

The total shear deformations of the SDT are considered as the sum of the shearing of the concrete segments plus the shear-induced offsets at the joints. The latter is herein accounted for by introducing the shear stiffness reduction ratio of the ring joint area  $\zeta_{Joint}$  (see Fig. 8). As expected, reducing the shear stiffness ( $\zeta_{Joint} < 1$ ) results in an increase of the differential displacements for loading as well as unloading conditions; see Fig. 12 and Fig. 13. The tendency towards increased differential displacements can be explained by additional translational movements at the ring joints (i.e. ring joint slipping). It can be further inferred from the results that the crown displacements are almost not affected for  $\zeta_{Joint}$ -values greater than or equal to 0.30. On the contrary, crown displacements are significantly influenced when the equivalent shear stiffness  $\zeta_{Joint}$  is smaller than 0.10 indicating a much softer longitudinal deformation behaviour. Since bending is considered the most relevant type of deformation with respect to tunnel linings [4], the definition of  $\zeta_{Joint}$  is particularly of importance, as  $\zeta_{Joint}$ -values smaller than 0.10 may overestimate the crown displacements significantly.

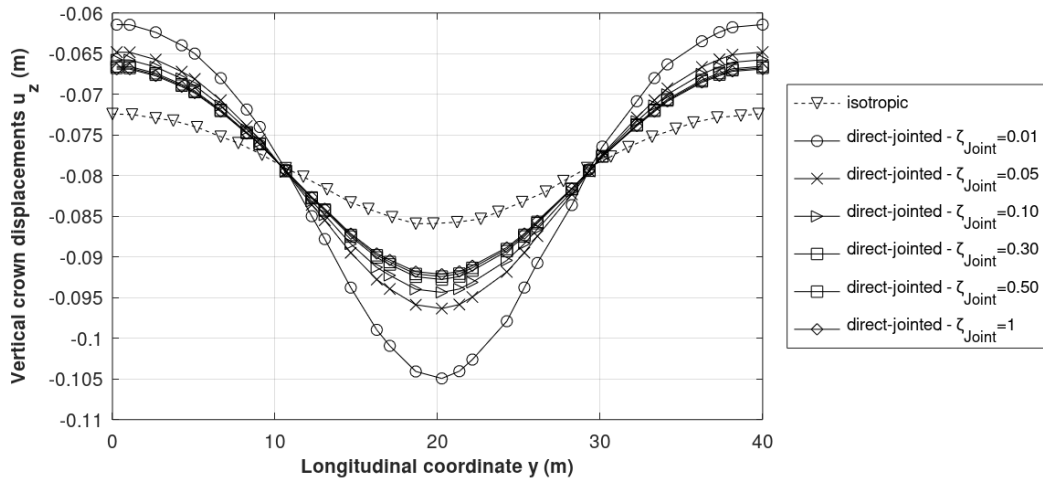


**Fig. 12.** Effect of shear stiffness reduction  $\zeta_{\text{Joint}}$  on the longitudinal distribution of vertical crown displacements (3D, loading).

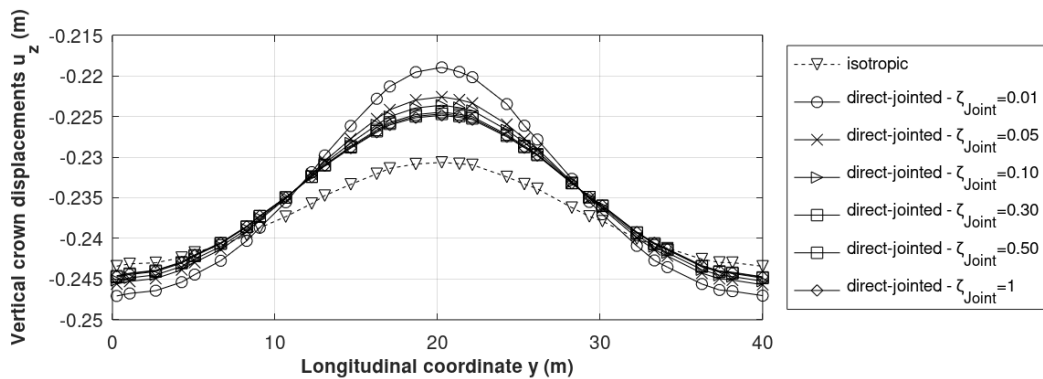


**Fig. 13.** Effect of shear stiffness reduction  $\zeta_{\text{Joint}}$  on the longitudinal distribution of vertical crown displacements (3D, unloading).

Regarding the max. cross-sectional bending moment  $M_{\text{max}}$  a similar tendency is observed as a consequence of reducing the shear stiffness in the ring joint area. When the lining is subjected to loading conditions, an increase of the shear stiffness leads to decreasing max. bending moments in the cross section as shown in Fig. 14. This shear stiffness dependence is observed for different constitutive models representing the soil behaviour. For the presented studies the HSS constitutive model [30] as well as linear elasticity have been used to model the soil, whereas it has to be addressed that the latter predicts lower variations of the max. bending moment. The obtained results agree also with the observations made in [27]. However, it has to be mentioned that the opposite tendency is observed when unloading conditions are considered; in other words, an increase in shear stiffness leads to higher max. bending moments. This again applies for different constitutive models. Thus, it can be concluded that the recommendations regarding structural measures for segmental tunnel linings presented by [27] are restricted to loading conditions (i.e. the shear resistance ability between rings should be increased in order to reduce the additional internal forces induced by ground displacement). Nevertheless, similar to what has been observed for the crown displacements, the max. bending moments are almost constant, if  $\zeta_{\text{Joint}}$ -values are set greater than or equal 0.30 (see Fig. 14).

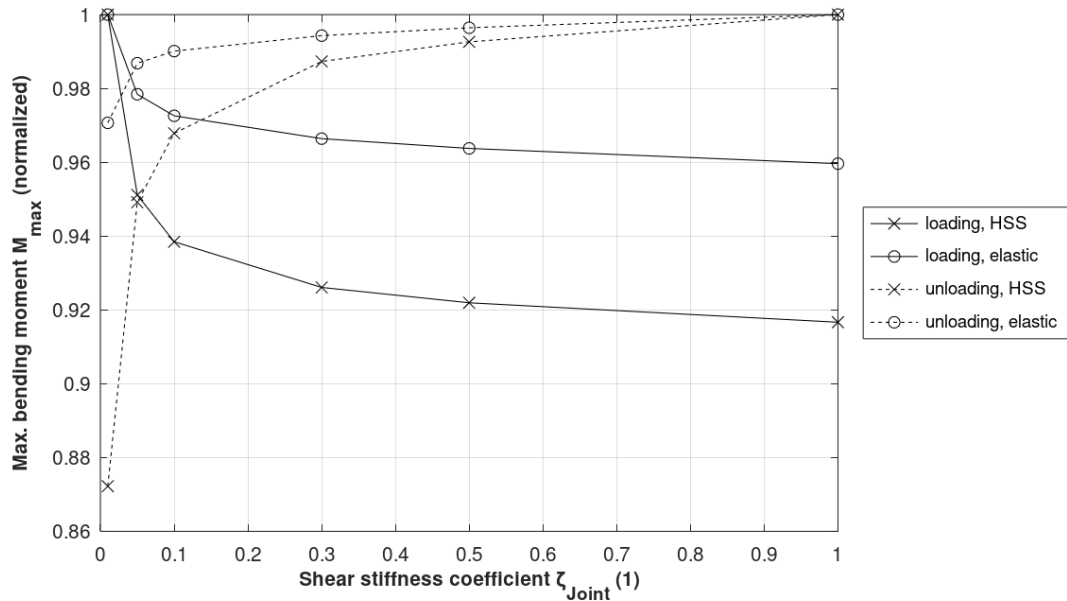


Fig. 14. Relationship between shear stiffness coefficient  $\zeta_{Joint}$  and max. cross-sectional bending moment  $M_{max}$  (normalized against the extreme value of  $M_{max}$  derived from the respective model).

### 5. Case study

The key observations of the preliminary studies are further applied to analyse the structural response of the existing drainage tunnel SDT to the construction of a suburban railway project conducted above the tunnel axis. The 3D FE model and some geometrical information are shown in Fig. 15. It also has to be mentioned that this project was executed by the cut-and-cover method. It was expected that the excavation activity below the roof slab would have a considerable effect on the behaviour of the subjacent SDT due to spatial boundary conditions. When the excavation base is reached, the remaining overburden approaches a minimum value of around 1 m, thereby invoking additional ground heave; a detailed description is given in [31].

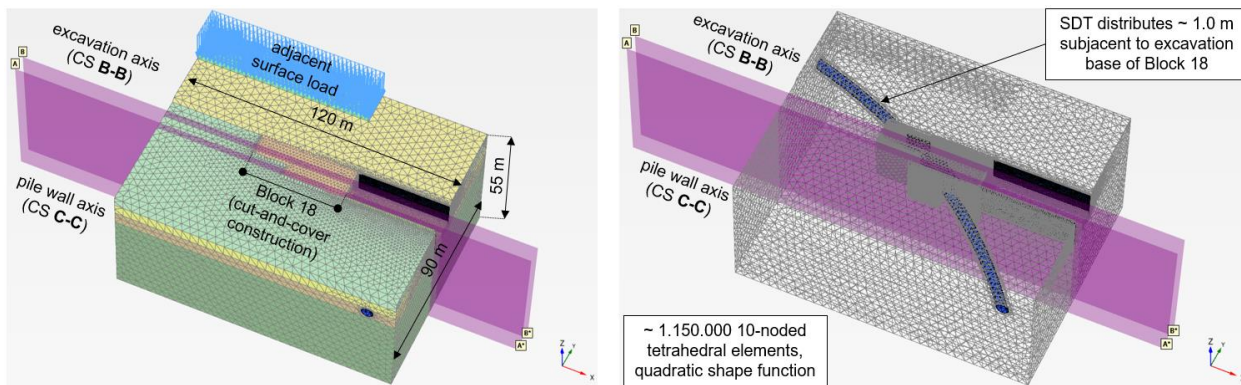


Fig. 15. Overview of entire 3D model (left) and 3D FE mesh (right).

In order to predict the deformation behaviour during the construction as realistic as possible, the SDT is modelled as indirect-model with anisotropic material. To define the input parameters for the segmental lining, the stiffness reduction ratios are defined in accordance with the

recommendations derived from the studies presented above; accordingly, the stiffness reduction factors are set to  $\eta = 1.0$  and  $\xi_{Cont.} = 0.24$ , respectively. Since the determination of the shear stiffness reduction would require a number of assumptions and, furthermore, varies among different loading conditions, this effect was not considered in the 3D FEA (see Fig. 14).

The following paragraph provides a comparison of the crown deformation occurring throughout the analysis of the construction process at different cross-sections (i.e. B-B and C-C). Fig. 16 shows both, the vertical phase displacements  $Pu_z$  as well as the total deformations  $u_z$ , related to the individual calculation phases. A closer inspection of the plotted data leads to the following findings:

- The max. total displacements ( $u_{z,B-B}$ : 36 mm,  $u_{z,C-C}$ : 24 mm) are observed after the final excavation sequence in Block 18 (i.e. Exc 3.3). The soil heave is more pronounced at the position of the excavation axis in cross-section B-B.
- The excavation of the working plane, which is referred to as “Dem” in Fig. 16, significantly affects the vertical crown displacements ( $Pu_{z,B-B}$ : 4 mm,  $Pu_{z,C-C}$ : 7 mm). This has to be taken into consideration when comparing the obtained results of the present 3D FEA with the results of on-site measurements.
- In both cross-sections, the max. phase displacements (heave) occur at the first excavation phase below the roof slab of Block 18 ( $Pu_{z,B-B}$ : 15 mm,  $Pu_{z,C-C}$ : 9 mm).
- The pre-tension phases (PreT: construction of the reinforced invert, pre-tensioning of the respective ground anchors) have a minor effect on the crown displacements ( $Pu_z < 0.8$  mm). However, they solely aim to prevent the tunnel lining from being subjected to tension during the final calculation phase.

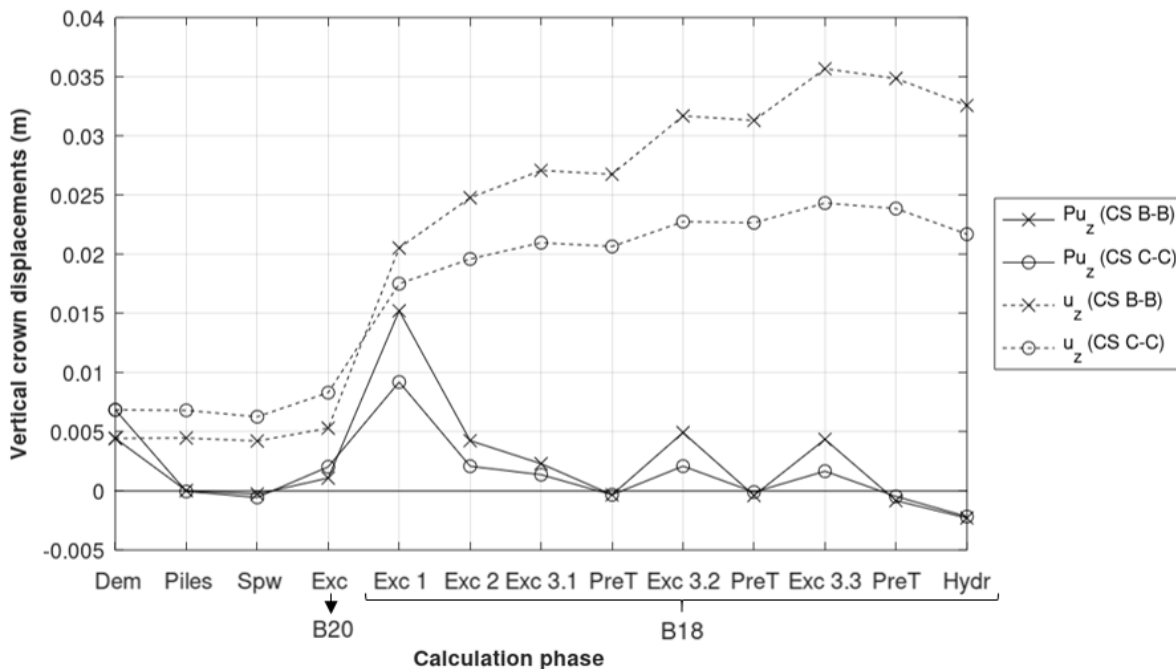


Fig. 16. Development of vertical crown displacements at different cross-sections.

## 6. Conclusions

Segmental joints significantly influence the structural behaviour of shield-driven tunnel linings since they decrease the lining stiffness; ignoring them may lead to a conservative design. On the contrary, overestimating the influence of joints and reducing the stiffness of a tunnel structure extensively could result in larger deformations; as a consequence, the level of waterproofness might be misinterpreted. Thus, the selection of realistic modeling parameters is an important, but difficult task during the analysis and design of segmental tunnel linings. In this context, the present paper investigates the influence of both, longitudinal joints as well as ring joints applying a hybrid modeling approach. The latter combines analytical solutions and numerical parameter studies. Therefore, the geometry of an existing segmental drainage tunnel (SDT) serves as reference structure. The presented numerical studies finally allow a more realistic estimation of the SDT modeling parameters and, thus, enable an improved modeling procedure. The key findings of the numerical investigations related to the hybrid modeling approach are as follows:

- Assuming a straight-jointed ring geometry composed of four segments and symmetrical loading conditions, the cross sectional behaviour of the SDT is hardly affected by its longitudinal joints. This holds true for both internal forces as well as lining deformations developing in circumferential direction. In other words, in the present case, the jointed cross section can be simplified as uniform ring which corresponds to an effective transversal bending rigidity ratio  $\eta = 1$ .
- Concerning the influence of ring joints on the behaviour of segmental linings, several analytical solutions exist which allow for a first-order approximation of the corresponding stiffness reduction in axial direction. It was found that the influence length of the ring joint plays a pivotal role in assessing the longitudinal bending rigidity  $\xi_{\text{Cont.}}$ . In the present case, the influence length is defined equal to the ring joint thickness which gives  $\xi_{\text{Cont.}} = 0.24$ .
- Considering the translational deformation of adjoining segments in the ring joint area by means of a shear-stiffness reduction, the results show that the max. cross sectional bending moments decrease with an increase in shear stiffness when the structure is subjected to loading conditions; this tendency is in agreement with results presented by [27]. However, an opposing tendency is observed when unloading conditions are considered. Hence, it seems that recommendations regarding the conceptual design of segmental tunnel linings presented by [27] are restricted to loading conditions. The results further underline the interaction between stiffness parameters in circumferential and longitudinal direction.

The presented findings of the hybrid modeling approach are further applied to a real boundary value problem to investigate the response of a shield-driven drainage tunnel to construction activities conducted above the tunnel structure. The obtained results allowed for the development of both, a cost-effective and safe construction program.

## References

- [1] German Tunnelling Committee (ITA-AITES), Recommendations for the selection of tunnelling machines, Cologne 2010.



- [2] Lee KM, Hou XY, Ge XW, Tang Y. An analytical solution for a jointed shield-driven tunnel lining. *Int J Numer Anal Methods Geomech* 2001;25:365–90. doi:10.1002/nag.134.
- [3] Zhang L, Feng K, Gou C, He C, Liang K, Zhang H. Failure tests and bearing performance of prototype segmental linings of shield tunnel under high water pressure. *Tunn Undergr Sp Technol* 2019;92:103053. doi:10.1016/j.tust.2019.103053.
- [4] Yu H, Cai C, Bobet A, Zhao X, Yuan Y. Analytical solution for longitudinal bending stiffness of shield tunnels. *Tunn Undergr Sp Technol* 2019;83:27–34. doi:10.1016/j.tust.2018.09.011.
- [5] Zhang J-L, Schlappal T, Yuan Y, Mang HA, Pichler B. The influence of interfacial joints on the structural behavior of segmental tunnel rings subjected to ground pressure. *Tunn Undergr Sp Technol* 2019;84:538–56. doi:10.1016/j.tust.2018.08.025.
- [6] German Tunnelling Committee (ITA-AITES), Recommendations for the design, production and installation of segmental rings, Cologne 2013.
- [7] Huang X, Huang H, Zhang J. Flattening of jointed shield-driven tunnel induced by longitudinal differential settlements. *Tunn Undergr Sp Technol* 2012;31:20–32. doi:10.1016/j.tust.2012.04.002.
- [8] Bakker KJ. Soil retaining structures: Development of models for structural analysis, PhD Thesis, Delft University of Technology 2000.
- [9] Blom CBM. Design philosophy of concrete linings for tunnels in soft soils, PhD Thesis, Delft University of Technology 2002.
- [10] Voit T. 3D - FEM Modelling of a Deep Excavation, Master’s Thesis, Graz University of Technology 2016.
- [11] Zdravkovic L, Potts DM, St John HD. Modelling of a 3D excavation in finite element analysis. *Géotechnique* 2005;55:497–513. doi:10.1680/geot.2005.55.7.497.
- [12] Teachavorasinskun S, Chub-uppakarn T. Influence of segmental joints on tunnel lining. *Tunn Undergr Sp Technol* 2010;25:490–4. doi:10.1016/j.tust.2010.02.003.
- [13] Gong C, Ding W, Soga K, Mosalam KM. Failure mechanism of joint waterproofing in precast segmental tunnel linings. *Tunn Undergr Sp Technol* 2019;84:334–52. doi:10.1016/j.tust.2018.11.003.
- [14] Do N-A, Dias D, Oreste P, Djeran-Maigre I. 2D numerical investigation of segmental tunnel lining behavior. *Tunn Undergr Sp Technol* 2013;37:115–27. doi:10.1016/j.tust.2013.03.008.
- [15] Granitzer A. 3D Finite Element Analysis of building lot “Wolframstraße”, Master’s Thesis, University of Leoben 2019.
- [16] Brinkgreve RBJ, Engin E, Swolfs WM. Plaxis 2D, Finite element code for soil and rock analyses, users manual. Rotterdam. Delft Univ Technol PLAXIS Bv 2012;14:320.
- [17] Brinkgreve RBJ. PLAXIS 3D–Finite Element Code for Soil and Rock Analyses: Users Manual–Anniversary Edition” 2016.
- [18] Fu J, Yang J, Klapperich H, Wang S. Analytical Prediction of Ground Movements due to a Nonuniform Deforming Tunnel. *Int J Geomech* 2016;16:04015089. doi:10.1061/(ASCE)GM.1943-5622.0000580.
- [19] Potts DM, Zdravković L, Addenbrooke TI, Higgins KG, Kovačević N. Finite element analysis in geotechnical engineering: application. vol. 2. Thomas Telford London; 2001.
- [20] Do NA. Numerical analyses of segmental tunnel lining under static and dynamic loads, PhD Thesis, University of Lyon 2014.

- [21] Guan Z, Deng T, Wang G, Jiang Y. Studies on the key parameters in segmental lining design. *J Rock Mech Geotech Eng* 2015;7:674–83. doi:10.1016/j.jrmge.2015.08.008.
- [22] Wood AMM. The circular tunnel in elastic ground. *Géotechnique* 1975;25:115–27. doi:10.1680/geot.1975.25.1.115.
- [23] Lee KM, Ge XW. The equivalence of a jointed shield-driven tunnel lining to a continuous ring structure. *Can Geotech J* 2001;38:461–83. doi:10.1139/t00-107.
- [24] SHIBA Y, KAWASHIMA K, OBINATA N, KANO T. An evaluation method of longitudinal stiffness of shield tunnel linings for application to seismic response analyses. *Doboku Gakkai Ronbunshu* 1988;1988:319–27.
- [25] Cui Q-L, Wu H-N, Xu Y-S, Shen S-L. Longitudinal deformation pattern of shield tunnel structure and analytical models: a review. *Japanese Geotech Soc Spec Publ* 2015;1:1–4.
- [26] Bao Z, YUAN Y, YU H, JI Q, ZUO F. Longitudinal rigidity of shield tunnels based on numerical investigation. *SEE Tunn. Promot. Tunneling SEE Reg. ITA WTC 2015 Congr. 41st Gen. Assem. Croat.*, 2015.
- [27] Liao S-M, Peng F-L, Shen S-L. Analysis of shearing effect on tunnel induced by load transfer along longitudinal direction. *Tunn Undergr Sp Technol* 2008;23:421–30. doi:10.1016/j.tust.2007.07.001.
- [28] Plaxis B V. *Plaxis, finite element code for soil and rock analyses*. RBJ Brinkgreve Delft, Netherlands 2002.
- [29] Murakanu H, Koizumi A. Study of load-bearing capacity and mechanics of shield segment ring. *Proc Japan Soc Civ Eng* 1978;1978:103–15. doi:10.2208/jscej1969.1978.272\_103.
- [30] Benz T. *Small-strain stiffness of soils and its numerical consequences*, PhD Thesis, University of Stuttgart 2006.
- [31] Summerer W, Hosp E. *Bergmännischer Aushub in Deckelbauweise Block 18: Statische Berechnung* 2018.